# Localization accuracy of sphere fiducials in computed tomography images

Jan-Philipp Kobler[a], Jesús Díaz Díaz[a], J. Michael Fitzpatrick[b], G. Jakob Lexow[c], Omid Majdani[c], Tobias Ortmaier[a]

[a]Leibniz Universität Hannover, Institute of Mechatronic Systems, Hannover, Germany;
[b]Vanderbilt University, Department of Electrical Engineering and Computer Science, Nashville, TN, USA
[c]Hannover Medical School, Department of Otolaryngology, Hannover, Germany;

## ABSTRACT

In recent years, bone-attached robots and microstereotactic frames have attracted increasing interest due to the promising targeting accuracy they provide. Such devices attach to a patient's skull via bone anchors, which are used as landmarks during intervention planning as well. However, as simulation results reveal, the performance of such mechanisms is limited by errors occurring during the localization of their bone anchors in preoperatively acquired computed tomography images. Therefore, it is desirable to identify the most suitable fiducials as well as the most accurate method for fiducial localization. We present experimental results of a study focusing on the fiducial localization error (FLE) of spheres. Two phantoms equipped with fiducials made from ferromagnetic steel and titanium, respectively, are used to compare two clinically available imaging modalities (multi-slice CT (MSCT) and cone-beam CT (CBCT)), three localization algorithms as well as two methods for approximating the FLE. Furthermore, the impact of cubic interpolation applied to the images is investigated. Results reveal that, generally, the achievable localization accuracy in CBCT image data is significantly higher compared to MSCT imaging. The lowest FLEs (approx. 40 µm) are obtained using spheres made from titanium, CBCT imaging, template matching based on cross correlation for localization, and interpolating the images by a factor of sixteen. Nevertheless, the achievable localization accuracy of spheres made from steel is only slightly inferior. The outcomes of the presented study will be valuable considering the optimization of future microstereotactic frame prototypes as well as the operative workflow.

**Keywords:** accuracy, fiducial localization error, medical image processing, surgical robotics

## 1. DESCRIPTION OF PURPOSE

Keyhole otologic surgery calls for specialized instrumentation to satisfy the demanding requirements with respect to accuracy and minimum trauma. Surgical robotics for use in this field must provide the surgeon with an instrument guidance of submillimetric accuracy.[1] In this context, minimally invasive cochlear implantation is often considered as a benchmark application. The aim of several research groups comprises drilling a single canal from the mastoid to the basal turn of the scala tympani[2–4] and inserting an electrode for stimulation of the auditory nerve.

Recently, so called microstereotactic frames have demonstrated a remarkably high targeting accuracy[5,6] in deep-brain stimulation and minimally invasive cochlear implantation. Such devices fasten rigidly to a patient's skull via bone anchors and provide instrument guidance during surgery. They use the anchors both as fiducials and base joints, and hence neither intraoperative navigation nor explicit point-based registration between patient and device is required. The StarFix™ (FHC, Inc., Bowdoin, ME, USA) is a passive, single-use, patient specific platform, manufactured using rapid prototyping based on preoperative trajectory planning. Even though it is clinically approved, the off-site fabrication of the platform results in an inconvenient, two day delay between preoperative imaging and surgical intervention. The Microtable, which represents a further development of the

Further author information: (Send correspondence to J.P.K.)
J.P.K.: E-mail: jan-philipp.kobler@imes.uni-hannover.de, Telephone: +49 (0)511 762 17840

Medical Imaging 2014: Image-Guided Procedures, Robotic Interventions, and Modeling,
edited by Ziv R. Yaniv, David R. Holmes III, Proc. of SPIE Vol. 9036, 90360Z
 · doi: 10.1117/12.2043472

StarFix™ system, was developed at the Vanderbilt University Medical Center (Nashville, TN, USA) for cochlear implantation.[7] Its platform is fabricated in less than four minutes using a computer numerical control (CNC) milling machine and sterilized prior to surgery.

Serving similar purpose, Kratchman et al. (members of Labadie's research group) proposed a bone-attached robot as a microstereotactic platform, which is mounted on a rigid pre-positioning frame.[8] Furthermore, a microstereotactic frame that is adjusted by a robot, immobilized, and then used as a tool guide in deep brain stimulation was investigated.[6] In this context, the authors propose a passive Stewart-Gough-Platform attached directly to bone anchors, eliminating the need for a rigid fixation frame, and, therefore, providing enhanced flexibility during the surgical procedure.[9] The performance criteria of the parallel robot are further increased by implementing reconfigurability and by exploiting redundant degrees of freedom of the mechanism during incision planning.

However, simulation results reveal that the performance of the parallel kinematic mechanism is significantly affected by errors occurring during the localization of its base joints in the preoperatively acquired CT scans.[9] Therefore, it is desirable to identify the most suitable fiducials as well as the most accurate localization method. In this context, the achievable localization accuracy is expected to depend on three major factors: the material of the spherical bone anchor heads, the imaging modality, and the applied localization algorithm. The material of the bone anchor heads plays a crucial role considering the choice of an appropriate fixation mechanism. In order to facilitate the intraoperative handling, a first prototype of the proposed robot is equipped with magnetic, spherical joints which enable a convenient assembly of the mechanism. This requires the spherical heads of the anchors to be made from a ferromagnetic material, e.g. steel, which is known to cause artifacts in the preoperative images. Using well established titanium spheres prohibits magnetic bearings, but results in fewer artifacts affecting the localization accuracy.

Being the major source of inaccuracies, errors in base joint localization need to be taken into account considering the design of future prototypes as well. This can be achieved by implementing a kinematic error model of the parallel mechanism, which provides an estimation of the overall achievable targeting accuracy.[10] A design optimization of the parallel robot to meet the challenging demands can then be performed. However, in order to obtain realistic results, the aforementioned formulation needs to be parameterized appropriately. Therefore, this contribution focuses on the achievable localization accuracy of spherical fiducials in CT scans, assessing available imaging modalities, fiducial materials, and localization algorithms.

## 2. METHODS

In the field of medical image registration, the Euclidean distance between true and measured location of a fiducial is commonly referred to as the *Fiducial Localization Error* (FLE) as introduced by Fitzpatrick et al.[11,12] According to the widely accepted error theory, the FLE cannot be measured directly since the true location of a fiducial is unknown. However, two methods for obtaining an approximation can be found in the literature. Both require non-collinear configurations of at least three fiducials. In case a ground truth measurement is available, the FLE can be estimated by registering identified fiducials in the image space to the ground truth (GT):

$$\mathrm{FLE}^2_{\mathrm{GT}} = \frac{N}{N-2}\mathrm{FRE}^2, \tag{1}$$

where $N$ denotes the number of fiducials and FRE denotes the *Fiducial Registration Error*, i.e., the root mean square displacement between the coordinates of corresponding fiducials after registration. If no ground truth measurement exists, an alternative approximation of the FLE can be obtained by performing an intramodal (IM) registration of two different CT scans of the same fiducial configuration. In that case,

$$\mathrm{FLE}^2_{\mathrm{image}} = \frac{1}{2}\frac{N}{N-2}\mathrm{FRE}^2. \tag{2}$$

The factor $1/2$ accounts for the fact that with IM registration $\mathrm{FRE}^2$ can be expected to be twice as large because localization error is present in both spaces. If $M$ independent registrations are performed, then the best estimate


Figure 1. a) Bone anchor with spherical head made from titanium, b) corresponding MSCT image, c) measurement phantom made from acrylic glass.

is:

$$\mathrm{FLE}^2_{\mathrm{image}} = \frac{N}{2M(N-2)} \sum_{m=1}^{M} \mathrm{FRE}^2_m, \tag{3}$$

where $\mathrm{FRE}_m$ is the FRE of the $m$-th registration.

The bone anchor used in this study is equipped with a cylindrical, bone cutting thread to ensure a rigid fixation within the skull (see Fig. 1). The spherical head, which serves as one base joint of the proposed parallel robot, is screwed onto an M 1.6 thread bar once the bone anchor is seated. Here, spheres having a diameter of 8 mm are chosen. The fiducial point to be localized is defined as the centroid of the sphere. In order to assess the impact of the fiducial material on the achievable localization accuracy, two acrylic phantoms containing bone anchors were made. One is equipped with eight spherical heads made from titanium, while a second phantom features nine spheres made from ferromagnetic steel. In both cases, the spheres are arranged in a circle having an approximate diameter of 80 mm.

Both phantoms were scanned in ten different poses (positions and orientations), each using two clinically available imaging modalities. On the one hand, MSCT imaging (LightSpeed16, GE Medical Systems, Little Chalfont, GB) with a resulting voxel size of 312.5 µm x 312.5 µm x 625 µm was performed. On the other hand, a flat-panel, cone-beam CT (CBCT) scanner (Xoran xCAT® ENT, Xoran Technologies, Ann Arbor, MI, USA) which provides an isotropic resolution of 300 µm x 300 µm x 300 µm has been employed. Further details regarding the parameters of the two imaging modalities are given in Tab. 1.

Table 1. Parameters of the employed imaging modalities.

| | GE LightSpeed 16 (MSCT) | Xoran xCAT® ENT (CBCT) |
|---|---|---|
| field of view | 16 cm x 16 cm x 16 cm | 21 cm x 21 cm x 14 cm |
| x-ray tube voltage | 100 kV | 120 kV |
| x-ray tube current | 80 mA | 6 mA |
| resulting voxel size | 312.5 µm x 312.5 µm x 625 µm | 300 µm x 300 µm x 300 µm |

A ground truth was obtained by measuring the fiducial configurations of each phantom ten times using a Faro Gage coordinate measuring machine (Faro Technologies Inc., Lake Mary, FL, USA). In order to identify the contribution to the localization error made by these measurements, $\mathrm{FLE}^2_{\mathrm{FARO}}$ was determined using the IM method described above and accounted for as follows:

$$\mathrm{FLE}^2_{\mathrm{image}} = \mathrm{FLE}^2_{\mathrm{GT}} - \mathrm{FLE}^2_{\mathrm{FARO}}. \tag{4}$$

Localization of the spherical fiducials in the computed tomography images is achieved by an automatic algorithm, which is preferred to a manual procedure since it minimizes errors introduced by human interaction. First, a coarse estimation of the sphere centroids is obtained through binarization of the image datasets and application of an edge-filter on each slice. Moreover, opening and closing is performed and small, connected regions are removed in order to distinguish the sphere fiducials from the bone anchors' bases. Finally, subvolumes encompassing one sphere each are cropped from the image datasets exploiting both the known number of fiducials and the sphere diameter. In order to precisely determine the fiducial positions, the subvolumes containing the spheres are fed to the following three algorithms, which are then compared with respect to the achievable accuracy:

- Matching of a sphere template to each image subvolume by cross correlation (CC).[13]
- Fitting a sphere to each image subvolume by solving a linear least-squares problem (LS).[14]
- Binarization, edge filtering and subsequent application of the Hough-Transform (HT) for detection of spheres.[15]

In order to localize the spheres at subvoxel resolution, cubic interpolation is optionally performed on the image subvolumes prior to applying the aforementioned algorithms. In this study, interpolation factors IF = {1;2;4;8;16} are compared to assess the influence on the achievable localization accuracy. Each identified fiducial configuration is finally compared to the ground truth (GT) using (1), being $N = 8$ and $N = 9$ for titanium and steel spheres, respectively. Furthermore, the IM approximation of the FLE is computed, where $M = 45$ for each investigated parameter combination.

## 3. RESULTS

Prior to processing the computed tomography datasets, a ground truth measurement of the fiducial configurations was obtained using a Faro Gage coordinate measuring machine according to the method described above. The data obtained during the experiments are given in Fig. 2. The value $\mathrm{FLE_{FARO}}$ is found to be 13.4 µm with the steel sphere phantom and 12.1 µm when the phantom equipped with titanium spheres is used. Even though the shapes of the spheres are similar, small differences between the $\mathrm{FLE_{FARO}}$ values result from the manual measurement procedure during which each fiducial needs to be accessed with the FARO probe. In the following evaluation, the respective values of $\mathrm{FLE_{FARO,steel}}$ and $\mathrm{FLE_{FARO,titanium}}$ are used to account for the contribution to the localization error according to (4).

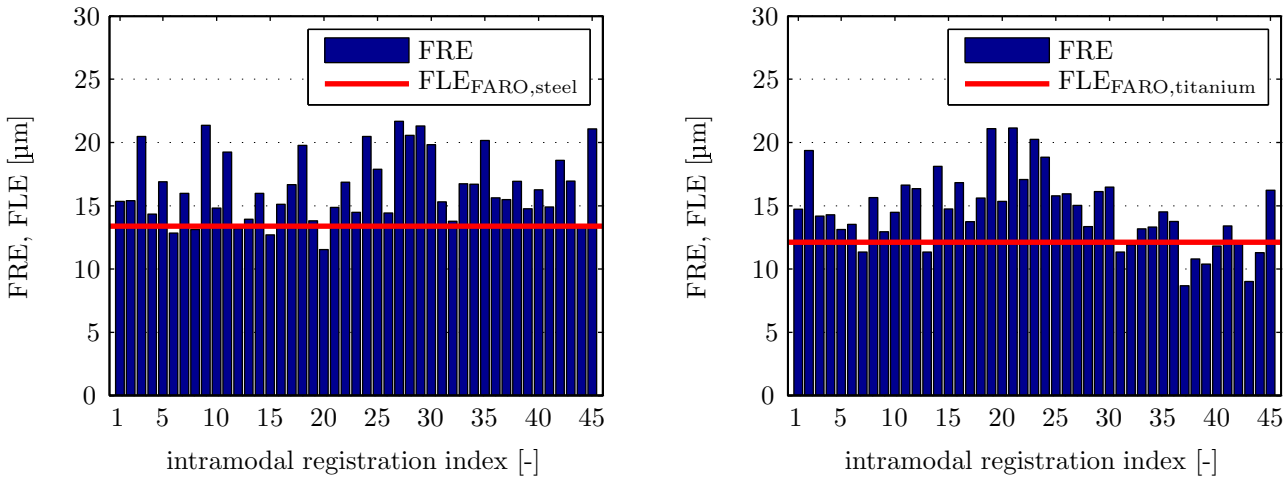


Figure 2. The value $\mathrm{FLE_{FARO}}$ is experimentally determined by measuring the fiducial configurations of the phantoms equipped with steel (left) and titanium (right) spheres ten times each. The FREs resulting from subsequent registrations are represented as blue bars while the red lines indicate the computed $\mathrm{FLE_{FARO,steel}}$ and $\mathrm{FLE_{FARO,titanium}}$, respectively.

The FLEs computed using the aforementioned evaluation methods are given in Table 2. Note that the FLE values for HT combined with interpolation factor 16 have been omitted due an unreasonably long computation time. Accurate localization of these fiducials depends on a determination of the average of the locations in the image of multiple points on its surface. Each voxel through which that surface passes provides such a point, and each suffers a vector error resulting from voxelation and noise. However, the fiducial is very large w.r.t. a voxel, and, therefore, the number of voxels through which the surface passes is very large – on the order of one to two thousand. While these errors are not completely independent, averaging them has the potential, as our results show, to reduce the fiducial localization error well below the voxel size.

Considering the MSCT scans, it is revealed that spheres made from steel are generally localized with higher accuracy compared to the spheres made from titanium. Furthermore, both interpolation factor and applied localization algorithm have a significant effect on the FLE estimates. For CC and HT, a high interpolation factor corresponds to high localization accuracy. However, improvements from interpolation factor 8 to interpolation factor 16 are comparably small, suggesting a saturation effect. Considering the LS algorithm, this saturation effect is present in the entire range of investigated interpolation factors. Therefore, cubic interpolation of the images provides no additional information beneficial to this kind of regression technique. If no interpolation is performed, i.e. IF=1, LS algorithm exhibits the best performance. Nevertheless, CC is able to outperform LS if the interpolation factor is equal or greater than 4. It is generally observed that the IM evaluation yields a FLE approximation which is very close to that of the ground truth registration. The lowest FLE, which is equal to the maximum achievable localization accuracy, is obtained using a sphere made from steel and CC at an interpolation factor of 16. The absolute values are 97.2 µm and 100.4 µm for the two evaluation methods, respectively.

In the image datasets obtained from a CBCT scanner, titanium spheres exhibit lower FLEs compared to spheres made from steel, which is especially the case considering the LS algorithm. If the interpolation factor is equal or greater than 2, the lowest FLE estimates are obtained using CC. The Hough Transform yields inconsistent results in both imaging modalities since the FLE increases if the interpolation factor changes from 2 to 4. Using CBCT imaging, the achievable localization accuracy of a sphere fiducial improves approximately by factor 2 compared to MSCT imaging, which is partly attributed to the smaller voxel size of the former. Here, the lowest FLE approximation is obtained using a sphere made from titanium and CC at interpolation factor 16. However, the measured FLE deviations due to the different sphere materials are comparably small being 12.4 µm and 9.9 µm for the two evaluation methods, respectively.

## 4. DISCUSSION AND CONCLUSION

In this study, the FLE of spheres in computed tomography was experimentally assessed. Results reveal that, for the employed phantoms, the achievable localization accuracy in CBCT image data is significantly higher compared to MSCT imaging. FLE approximations obtained using a ground truth measurement are slightly

Table 2. Experimentally determined values of $FLE_{image}$, given in µm, and corresponding parameter combinations.

| | | **Imaging Modality / Fiducial Material / Evaluation Method** | | | | | | | |
|---|---|---|---|---|---|---|---|---|---|
| **IF** | **Algorithm** | MSCT Steel IM | MSCT Titanium IM | MSCT Steel GT | MSCT Titanium GT | CBCT Steel IM | CBCT Titanium IM | CBCT Steel GT | CBCT Titanium GT |
| 1 | CC | 191.7 | 207.0 | 192.7 | 203.7 | 160.9 | 156.7 | 170.8 | 155.4 |
| | LS | 100.4 | 151.3 | 102.8 | 157.0 | 273.7 | 116.0 | 354.5 | 129.4 |
| | HT | 410.1 | 341.4 | 403.5 | 352.5 | 577.2 | 434.6 | 600.3 | 432.5 |
| 2 | CC | 128.3 | 141.1 | 129.1 | 148.5 | 90.2 | 78.9 | 90.7 | 86.3 |
| | LS | 101.8 | 148.4 | 104.0 | 154.3 | 263.2 | 117.0 | 339.8 | 130.4 |
| | HT | 181.1 | 238.7 | 188.3 | 246.4 | 276.2 | 86.5 | 289.0 | 87.1 |
| 4 | CC | 97.8 | 127.5 | 102.3 | 136.0 | 61.8 | 55.2 | 66,9 | 59.8 |
| | LS | 101.6 | 147.8 | 103.8 | 153.7 | 261.6 | 117.3 | 337.3 | 130.8 |
| | HT | 192.0 | 252.6 | 199.0 | 265.1 | 326.2 | 134.7 | 344.9 | 132.4 |
| 8 | CC | 99.6 | 125.0 | 101.8 | 134.3 | 50.4 | 41.4 | 54.2 | 50.3 |
| | LS | 101.6 | 147.5 | 103.8 | 153.4 | 260.0 | 117.5 | 334.7 | 131.0 |
| | HT | 190.1 | 254.9 | 199.5 | 266.9 | 251.2 | 73.1 | 257.4 | 75.1 |
| 16 | CC | 97.2 | 121.9 | 100.4 | 130.7 | 50.0 | 37.6 | 55.2 | 45.3 |
| | LS | 101.6 | 147.4 | 103.8 | 153.3 | 259.5 | 117.6 | 333,9 | 131.1 |
| | HT | - | - | - | - | - | - | - | - |

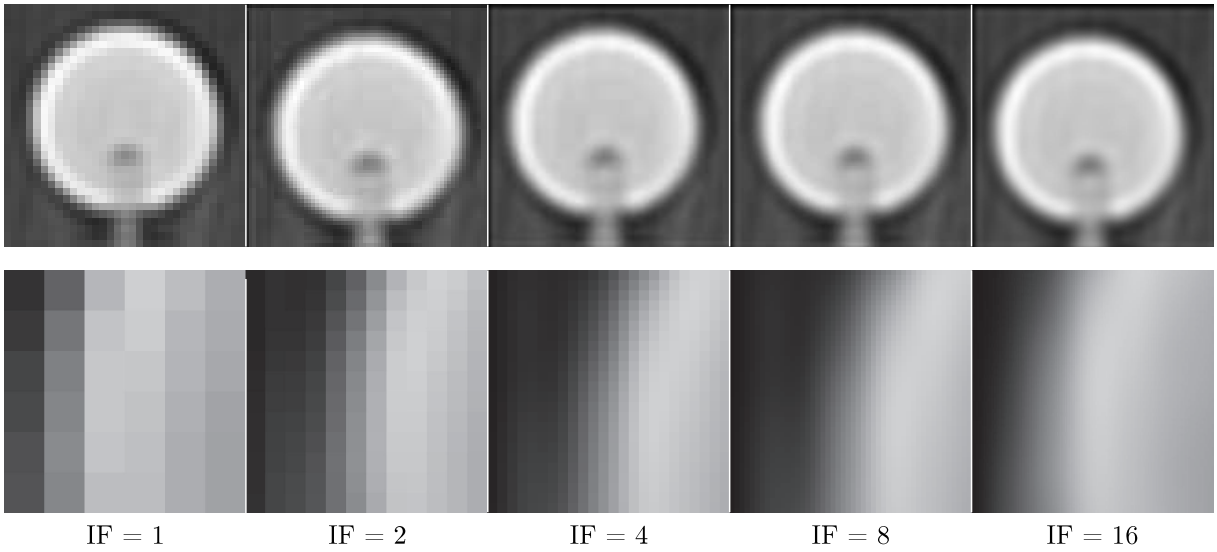


Figure 3. Cubic interpolation applied to two-dimensional slices of MSCT images. The effect is illustrated using the examples of one entire titanium sphere (top) and a section of one steel sphere having the dimensions of 6 x 6 pixels.

more conservative compared to intramodal registration. The CC algorithm combined with cubic interpolation was found to be most suitable for accurate localization once the interpolation factor was equal or greater than 4. As a result of the interpolation procedure, the FLEs are reduced well below the voxel sizes of the employed imaging modalities.

The absolute FLE values are considerably lower compared to those previously reported.[11,16] Geometrical distortion may be present to some degree in any imaging modality, and, as a result, the true FLEs may be somewhat smaller than our measured values. The measure FLE is increased, not because of a change in the shape of the fiducial itself, but because the overall fiducial configuration will differ from the true configuration. The resulting displacements of the fiducials from their true positions will be erroneously added to the measured FRE, which in turn inflates the calculated FLE. The smaller values for intramodal measurements (IM) in Table 2 as compared to the intermodal measurements (GT) suggest that there may be some geometrical distortion in one or both modalities, and given the high accuracy of the FARO system, the distortion is likely to be in the images. Smaller geometrical effects arise for intramodal measurement when (a) the orientation of the configuration is similar in the registered images and/or (b) there is an appreciable isotropic scaling. In those cases, the distortion varies weakly or not at all between the two images and therefore has little or no effect.

Regarding the design of the proposed, bone attached robot, a decision concerning the base joints can be made according to the obtained results. Furthermore, the obtained FLE values can be used to establish a precise kinematic error model of the parallel mechanism. Ongoing work is focused on investigating how other relevant parameters, e.g. the diameter of the sphere, influence the localization accuracy.

## REFERENCES

[1] Schipper, J., Aschendorff, A., Arapakis, I., Klenzner, T., Teszler, C. B., Ridder, G. J., and Laszig, R., "Navigation as a quality management tool in cochlear implant surgery," *J Laryngol Otol* **118**, 764 – 770 (10 2004).

[2] Eilers, H., Baron, S., Ortmaier, T., Heimann, B., Baier, C., Rau, T. S., Leinung, M., and Majdani, O., "Navigated, robot assisted drilling of a minimally invasive cochlear access," in [*Proc. IEEE Int. Conf. Mechatronics*], (2009).

[3] Balachandran, R., Mitchell, J. E., Blachon, G., Noble, J. H., Dawant, B. M., Fitzpatrick, J. M., and Labadie, R. F., "Percutaneous cochlear implant drilling via customized frames: an in vitro study," *Otolaryngology - Head and Neck Surgery* **142**, 421 – 426 (Mar. 2010).

[4] Bell, B., Stieger, C., Gerber, N., Arnold, A., Nauer, C., Hamacher, V., Kompis, M., Nolte, L., Caversaccio, M., and Weber, S., "A self-developed and constructed robot for minimally invasive cochlear implantation," *Acta Otolaryngol* **132**(4), 355 – 360 (2012).

[5] Balachandran, R., Mitchell, J., Dawant, B., and Fitzpatrick, J., "Accuracy evaluation of microtargeting platforms for deep-brain stimulation using virtual targets," *IEEE T. Bio-Med. Eng.* **56**(1), 37 – 44 (2009).

[6] Kratchman, L. B. and Fitzpatrick, J. M., "Robotically-adjustable microstereotactic frames for image-guided neurosurgery," in [*Proc. SPIE 8671, Medical Imaging*], (2013).

[7] Labadie, R. F., Mitchell, J., Balachandran, R., and Fitzpatrick, J. M., "Customized, rapid-production microstereotactic table for surgical targeting: description of concept and in vitro validation," *Int J CARS* **4**(3), 273 – 280 (2009).

[8] Kratchman, L. B., Blachon, G. S., Withrow, T. J., Balachandran, R., Labadie, R. F., and Webster, R. J., "Design of a bone-attached parallel robot for percutaneous cochlear implantation," *IEEE T. Bio-Med. Eng.* **58**, 2904 – 2910 (Oct. 2011).

[9] Kobler, J.-P., Kotlarski, J., Öltjen, J., Baron, S., and Ortmaier, T., "Design and analysis of a head-mounted parallel kinematic device for skull surgery," *Int J CARS* **7**(1), 137 – 149 (2012).

[10] Patel, A. and Ehmann, K., "Volumetric error analysis of a stewart platform-based machine tool," {*CIRP*} *Annals - Manufacturing Technology* **46**(1), 287 – 290 (1997).

[11] Maurer, Jr., C. R., McCrory, J. J., and Fitzpatrick, J. M., "Estimation of accuracy in localizing externally attached markers in multimodal volume head images," in [*Proc. SPIE 1898, Medical Imaging*], 43 – 54 (1993).

[12] Fitzpatrick, J. M., Hill, D. L. G., and Maurer, Jr., C. R., [*Handbook of Medical Imaging*], SPIE Press (2000).

[13] Guizar-Sicairos, M., Thurman, S. T., and Fienup, J. R., "Efficient subpixel image registration algorithms," *Opt. Lett.* **33**(2), 156 – 158 (2008).

[14] Coope, I. D., "Circle fitting by linear and nonlinear least squares," *J. Optim. Theory Appl.* **76**, 381 – 388 (1993).

[15] Illingworth, J. and Kittler, J., "A survey of the Hough transform," *Comput. Gr. Image Process.* **44**(1), 87 – 116 (1988).

[16] Gerber, N., Gavaghan, K., Bell, B., Williamson, T., Weisstanner, C., Caversaccio, M., and Weber, S., "High-accuracy patient-to-image registration for the facilitation of image-guided robotic microsurgery on the head," *IEEE T. Bio-Med. Eng.* **60**(4), 960 – 968 (2013).